Journal of Magnetism and Magnetic Materials 449 (2018) 68–76

Contents lists available at ScienceDirect

Journal of Magnetism and Magnetic Materials

journal homepage: www.elsevier.com/locate/jmmm

Research articles

Ferromagnetic resonance of 2D array of magnetic nanocaps

M.V. Sapozhnikov [a,*], L.I. Budarin [b], E.S. Demidov [b]

[a] Institute for Physics of Microstructures RAS, Nizhny Novgorod GSP-105, Russia
[b] N.I. Lobachevskii State University, Nizhny Novgorod 603950, Russia

ARTICLE INFO

Article history:
Received 28 April 2017
Received in revised form 6 September 2017
Accepted 28 September 2017
Available online 30 September 2017

Keywords:
Ferromagnetic resonance
Magnetic properties of nanostructures
Nonreciprocity
Curved magnetic surface

ABSTRACT

Nanostructured Co and permalloy films are fabricated on top of a polymethyl methacrylate (PMMA) colloidal crystals by magnetron sputtering. The influence of the geometry of the samples on the ferromagnetic resonance spectra is studied. A number of spin-wave resonances are found in the nanostructured system, while only a single resonance is observed in the spatially uniform flat film. The number of the observed resonance peaks increases with both the period of the colloidal crystal (120 ÷ 340 nm) and the film thickness (20 ÷ 90 nm). The micromagnetic simulations of the system show that the excited spin-wave modes are nonreciprocal because of nonzero toroidal momentum of the magnetization of the system.

1. Introduction

The progress of nanotechnology in recent years has triggered a wave of interest to magnonics. The focus point of the research is the application of the traditional concept of spin waves to the novel lines of investigation such as physics of artificial crystals, ultrafast magnetization dynamics or localized magnetic excitations [1]. The rising interest is caused by the potential ability of the spin waves to carry and process information on the nanoscale. Nanostructuring of magnetic systems provides a new degree of freedom connected with an artificial inhomogeneity in the magnetic field distribution [2]. Periodically structured magnetic materials play the special role as the spatial periodicity can be used for additional controlling propagation and scattering of spin waves [3]. Besides, the high-frequency localized excitations in magnetic structures are also subject to a growing interest in the field of nanomagnetism [4,5].

The methods to fabricate nanostructured magnetic materials commonly are different top-down lithographic techniques [6]. Unfortunately, they are usually slow and cost ineffective for mass production. On the other hand, bottom-up self-assembly method, such as metal deposition on the surface of colloidal crystal [7], allow to fabricate regular 2D lattices of magnetic nanocaps (i.e. hemispheres) [8,9]. In comparison with traditional flat 2D nanostructures the magnetic nanocaps is also some kind of extension of a nanostructure in the third dimension. It is a general trend in recent time [2]. It is known that static properties of the magnetic films on the top of colloidal crystals depend on the ratio of the particle diameter and the deposited film thickness [10–12]. If the thickness of the deposited film is comparable with the diameter of the colloidal particles, it is the topographically modulated continuous film. If the deposited film is thinner, it is rather the lattice of the connecting hemispherical nanocaps. The FMR properties of permalloy (Py) sample of the first type were recently studied [13] and two modes of the magnetization oscillations were found. The studied sample had a fixed film thickness and the fixed diameter of the particles of the substrate. Namely, 100-nm-thick Py film was sputtered onto a colloidal crystal with individual sphere radius of the 100 nm. Besides, only the field-in-plane geometry was studied. In the presented work we report on experimental study of the FMR properties of samples of the second type (the sputtered film is thinner than particle diameter) in the wide range of the geometrical parameters. Both in-plane and perpendicular orientations of the external magnetic field are investigated. The size of the particles of the substrate determines the period of the structure. It is varied in the limits of 120 ÷ 340 nm. The diameter of the particles determines the curvature of the surface of the magnetic nanocaps as well. It also can effect sample properties. The deposited magnetic film thickness is varied from 20 to 90 nm. We study both Co and Py samples. Co and Py are chosen as they have significantly different material parameters (magnetization and exchange coefficient) which should also effect the FMR properties. Several resonances are found in the FMR spectra. Their number has a tendency to increase both with the period and with the film thickness increase. Numerical micromagnetic modeling is used to simulate the structure of the resonant modes. It indicates that excited FMR oscillations can have a form of the nonreciprocal spiral spin waves running around the nanocap.

* Corresponding author.
E-mail address: msap@ipmras.ru (M.V. Sapozhnikov).

https://doi.org/10.1016/j.jmmm.2017.09.082
0304-8853/

2. Sample preparation and experimental details

Three-dimensional PMMA colloidal crystals are used as a substrate for the metal film deposition. The colloidal crystal samples are obtained through collaboration with Prof. B.B. Troitskii (G.A. Razuvaev Institute of Organometallic Chemistry RAS, Nizhny Novgorod, Russia). The synthesis of the colloidal crystals is described in [14] in detail. The particles forming the crystal are highly monodisperse, their diameter (D) is 120 ÷ 340 nm for the different samples.

The morphology of the samples is studied by scanning electron microscopy (SEM) before and after metal film deposition. The field emission scanning electron microscope with a Schottky Field emissions gun is used during this investigation. The topography of uncoated PMMA colloidal crystals is studied using SEM Supra 50VP (Carl Zeiss) in low-vacuum mode or in low-voltage mode (primary electron energy beam is 1–2.5 kV). The SEM images show that PMMA particles are densely packed in a hexagonal structure (Fig. 1a). The accuracy of the particles diameter measurements is 10% according to the instrument specification. The surface of the colloidal crystal is formed by crystallites with different in-plane orientations of the crystal axes. The typical crystallite size is 10–50 μm (Fig. 1b).

Ferromagnetic nanostructures are prepared by magnetron sputtering of the thin Co or Py layer on the surface of the PMMA colloidal crystal. Sample series with a nominal thickness (h) in the range from 20 to 90 nm is fabricated. The accuracy of the film manufacturing during the magnetron spattering on the flat surface for its thickness is ±15%. Magnetron current is 100 mA, target diame-

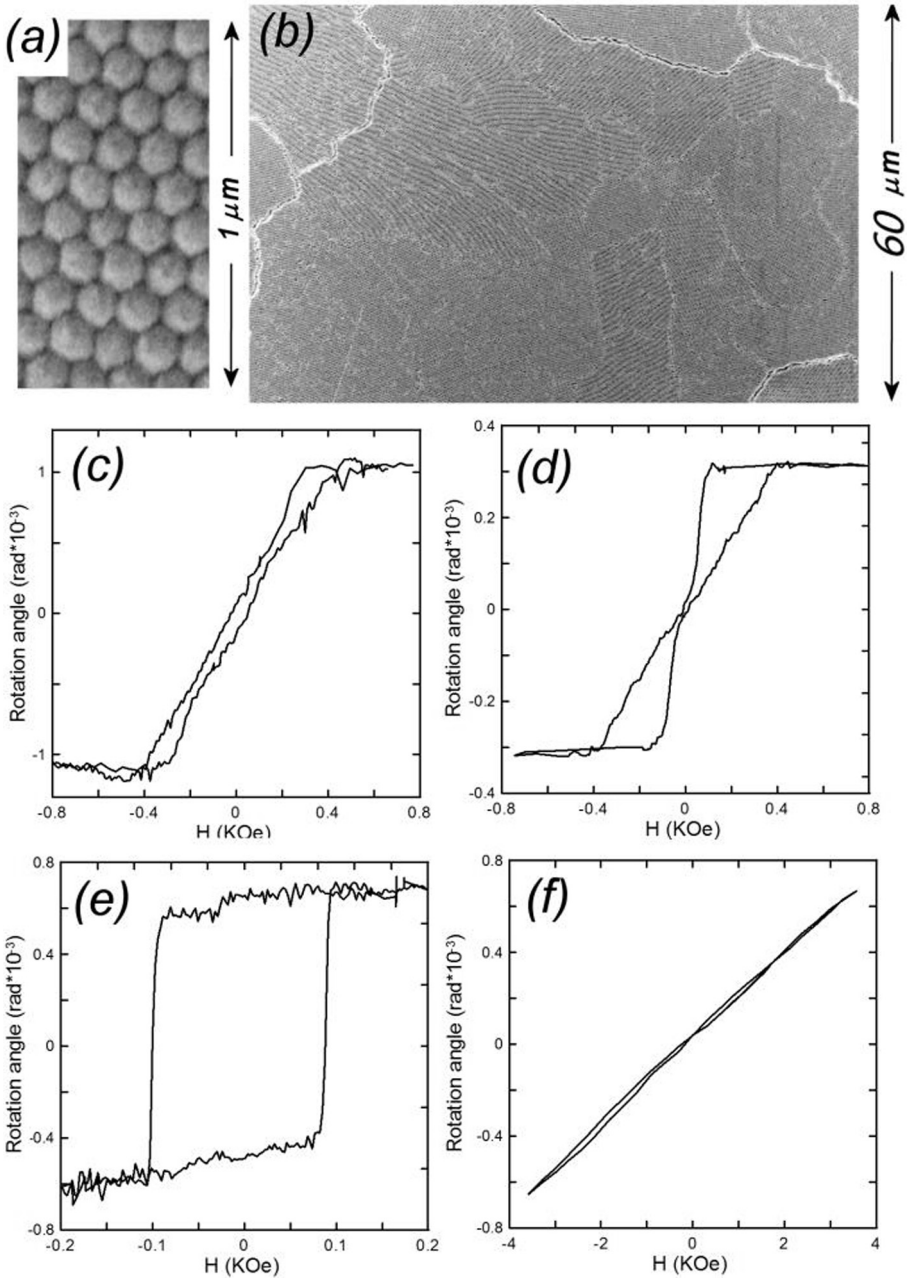

Fig. 1. a) SEM image of the 30 nm Co film on the top of the colloidal crystal, the period is 120 nm, the near-range order is visible. b) SEM image of the larger area of the colloidal crystal surface, different crystallites are visible due to different moiré. c)–f) Typical magnetization curves of the samples measured by MOKE. The parameters of the samples are the following: c) Co, D = 340 nm, h = 60 nm, in-plain field configuration; d) Co, D = 340 nm, h = 30 nm, in-plain field configuration; e) Co, D = 120 nm, h = 30 nm, in-plain field configuration; f) Py, D = 340 nm, h = 90 nm, perpendicular to the plain field configuration.

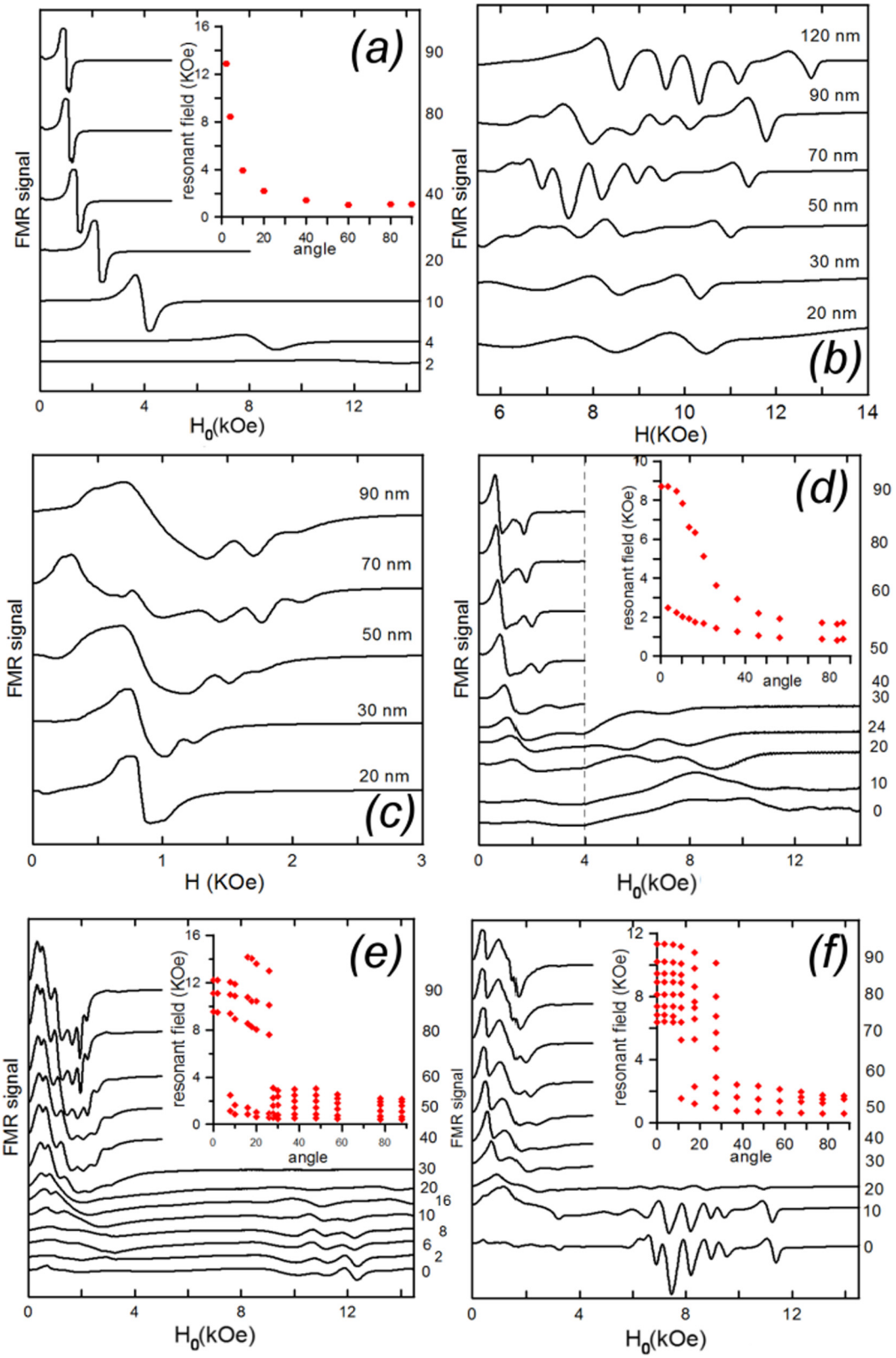

Fig. 2. FMR spectra (the first derivative of the electromagnetic field absorption) for the magnetic films deposited on the top of the colloidal crystal. The spectral curves are vertically shifted for better visibility. The insets represent the angular dependences of resonance field. a) The flat 30 nm Co film. The angle of the applied static field H with respect to the film normal is denoted at the right. b) The Py films of the different thickness deposited on the top of the colloidal crystal (D = 340 nm). The spectra for the perpendicular orientation of the static external field are represented. e) The Co films of the different thickness deposited on the top of the colloidal crystal (D = 340 nm). The spectra for the for the in-plane orientation of the static external field are represented. d) 50 nm Co film, colloidal particles diameter is 120nm. Different orientations of the static magnetic field in the respect to the normal are represented. e) 70 nm Co film, colloidal particles diameter is 340nm. Different orientations of the static magnetic field are represented. f) 70 nm Py film, colloidal particles diameter is 340nm. Different orientations of the static magnetic field are represented.

ter is 60 mm, the distance between the target and substrate is 150 mm. Pressure of the Ar atmosphere during the sputtering is 2×10^{-3} Torr, the corresponding mean free path is 120 mm, which is comparable with the target-substrate distance. Additional 2-nm-thick Si layer is deposited to prevent oxidation. As the result, the colloidal particles are hemispherically covered with ferromagnetic layer and the obtained nanostructured film is the hexagonal close-packed array of the ferromagnetic nanocaps.

Evidently, the colloidal crystal template dictates the period of the magnetic system. Thus, a series of the samples with the different periods and thicknesses are prepared. It is necessary to note, that the referred above thicknesses are the thicknesses of the control Co or Py films on flat Si substrate prepared in the same run. The actual average thickness of the obtained ferromagnetic coating of a colloidal particle in radial direction is twice smaller (as the ratio of the surface area of hemisphere to the surface area of its supporting circle is equal to 2) and can be nonuniform.

The FMR measurements of the samples are performed with Bruker EMX Plus-10/12 spectrometer equipped by a dc magnet with field up to 15 KOe. Microwave magnetic field (H_{rf}) is perpendicular to the constant magnetic field (H_0) and has 9.85 GHz frequency. Its mode in the resonant cavity is TE011. During the measurements we sweep the magnitude of the constant magnetic field to obtain FMR spectrum. The sample is also rotated around the axis parallel to the direction of magnetic component of microwave field to investigate angular dependences of resonant fields. The measured FMR spectrum is the first derivative of the electromagnetic field absorption.

The static magnetization curves of the samples are obtained using Magneto-optic Kerr effect (MOKE) measurements in the fields up to 4KOe. The typical magnetization loops are represented in Fig. 1. In the case of the in-plain field configuration the Co caps exhibit the loop corresponding to the formation of the magnetic vortices (Fig. 2d), single domain states (Fig. 1e) or some mixture of these states depending on the sample parameters [10]. The arrays of the Py nanocaps demonstrate similar magnetization behavior [12]. In the perpendicular to the plain field configuration magnetization curves do not demonstrate hysteretic behavior (Fig. 1f).

3. Experimental results

In the studied range of the applied fields (0–15 KOe) the FMR spectra of the spatially uniform flat Co or Py films with the thickness of 10–90 nm have one peak. It corresponds to the uniform precession of the magnetization (Fig. 2a, se also [15] and references therein). Thicker film (>200 nm [16]) is necessary to excite non-uniform oscillation. The situation is drastically changes in the case of the magnetic films deposited on the surface of the colloidal crystal. The typical FMR spectra measured in this case are represented in Fig. 2. The main observed experimental results are the following:

(1) The FMR properties of the samples do not depend on the in-plain orientation of the constant magnetic field. While the individual colloidal crystal crystallite has hexagonal symmetry, the whole sample (1 mm^2) is isotropic in plane as it contains crystallites with any orientation of the axes. Therefore, the measurements are actually an angular average of numerous grains.
(2) The single resonance peak is still observed for the thinnest ferromagnetic films (20 nm thick) in the case of the in-plane orientation of the external field. The same result for the thin magnetic film on the top of the colloidal crystal was previously reported in Ref. [17].
(3) The number of the peaks increases with the increasing diameter of the colloidal particles.
(4) The number of the peaks increases with the increase of the ferromagnetic film thickness up to 70 nm (Fig. 2b, c) as well.
(5) The further increase of the film thickness (up to 90 nm) leads to decrease of the resonance peak number (Fig. 2b, c, Table 1).
(6) The effects are qualitatively the same for the Co and Py films. The difference is that the peaks are more pronounced for the in-plane external field orientation for the Co films (Fig. 2e) and for the perpendicular field configuration in the case of the Py films (Fig. 2f). The maximum number of the resonances for the Co nanocap arrays is 6. It is observed for the 70 nm thick film in the case of 340 nm colloidal particles for the in-plane orientation of the external field (Fig. 2e). The same sample with the Py film demonstrated 8 resonances when the field is perpendicular to the sample (Fig. 2f). These data are also tabulated in Table. 1. We should note that the resonant peaks are better pronounced for the field directed in-plane or perpendicularly to the plane. For the intermediate angles of the field directions, the number of the peaks is less and they are visible worse. In the case of the in-plane field configuration the measured resonance values of the external field are higher than the typical field of the magnetic vortex nucleation in the nanocap (50–100 Oe, Fig. 1d). So all observed resonances take place when the system is in the quasi-uniform magnetization state. The corresponding magnetization configuration obtained by micromagnetic simulations is represented in Fig. 7 also.

4. Micromagnetic simulation

In order to understand what types of the FMR modes can be excited in the lattices of the magnetic nanocaps, we carry out

Table 1
The number of the observed resonances for different colloidal particle diameter and the film thickness.

Colloidal crystal period (nm) ↓	Magnetic film thickness (nm)					
	20	30	50	70	90	120
In-plane field/Co film						
120	1	2	2	2	2	2
270	1	2	3	4		
340	1	2	3	6	3	
In-plane field/Py film						
340	1	1	2	2	3	
Perpendicular field/Co film						
120	2	1	1	1		
Perpendicular field/Py film						
120	2	1	1			
340	2	2	4	8	7	5

micromagnetic simulations utilizing the OOMMF code [18]. This code is based on a numerical solution of the system of Landau–Lif shitz–Gilbert (LLG) equations for the magnetization. The geometry of the simulated system is represented in Fig. 3a. It is the rectangular part of the hexagonal lattice of the magnetic nanocaps having the size of two elementary cells. Its sides are equal to D and $3^{1/2}D$, where D is a diameter of the nanocap. The simulated cell contains a whole hemisphere in the center and a quarter of the hemisphere in each corner. Such geometry of the cell is chosen because it can be periodically extended to form infinite 2D hexagonal lattice of the nanocaps. The demagnetizing fields of separate magnetic hemisphere and demagnetizing fields of 2D lattice of such hemispheres are very different, therefore, the usage of the periodical boundary conditions is necessary. While we knows the shape of the substrate formed by the periodically arranged spheres (the PMMA particles in the experiments), we do not exactly know how the magnetic material is distributed on the surface of the sphere. Two limiting cases can be considered. The first is if the magnetic material has the constant thickness ΔR in the radial direction (Fig. 3b). The second one takes a place if the magnetic material has the constant thickness h in the vertical (z) direction. Evidently $h = 2\Delta R$ (if $\Delta R << R$) for the same amount of the magnetic material. We will refer h or $2\Delta R$ as the effective thickness. We also refer these models as "ΔR-model" and "h-model" below.

We simulate the systems with the following geometrical parameters: hemisphere diameter $D = 120 \div 340$ nm; h, $2\Delta R = 20 \div 80$nm, grid size is 5 nm. We use the material parameters corresponding to bulk Py and Co. For Py exchange constant A is 1.3×10^{-6} erg/cm, saturated magnetization M_s is 860 emu/cm^3. For Co $A = 3.0 \times 10^{-6}$ erg/cm, $M_s = 1400$ emu/cm^3. We omit magnetic anisotropy, assuming polycrystalline structure of the metal coating [19,20]. The above material parameters correspond to the material parameters of the bulk samples, while the magnetization and exchange constant in the thin magnetic films on the surface of the PMMA can be different. Also, we do not have the accurate information of the magnetic material distribution over the sample surface, only the average thickness can be estimated. In this situation, the main purpose of the simulation is to understand the reason of the multiple resonances observed in the magnetic nanocap arrays. We also tried to find the same qualitative tendencies in the FMR dependency on the sample geometry in the experiment and simulations.

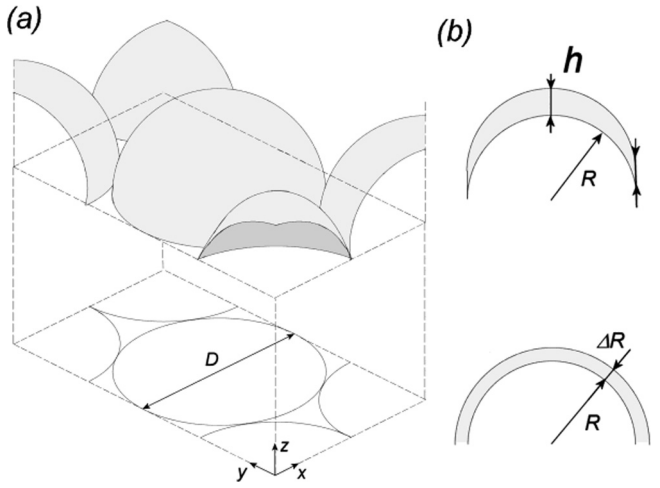

Fig. 3. a) The geometry of the simulated system. The perpendicular cell containing a whole hemisphere and the four quarters of the hemisphere can be periodically extended to form infinite 2D hexagonal lattice. b) The possible geometries of the film covering hemisphere.

5. Perpendicular external field configuration

Actually, the surface of the colloidal crystal is formed by crystallites with different orientations of the in-plane crystal axes (Fig. 1b). Nevertheless, if the constant external field is perpendicular to the surface, the orientation the in-plane crystal axes do not effect the resulting effective field. Therefore, the resonant frequencies and the magnetization oscillation modes is the same in all crystallites. The alternating RF field is perpendicular to the external constant field and is oriented in the plane of the array. Its orientation in the respect to the in-plane crystal axes can effect the amplitude of the FMR oscillations due to the different values of the overlap integral in these cases, but it do not effect the FMR spectra or on the structure of the oscillation modes. So our model is appropriate to such geometry. In our simulations the high frequency field (9.85 GHz) has the amplitude of 10 Oe and is oriented along x-axis ($\mathbf{H}_{rf} = H_{rf}\mathbf{x}_0$, Fig. 3a). The constant field ($\mathbf{H}_0 = H_0\mathbf{z}_0$) is swept from 16 kOe to −16 kOe. The field sweeping rate is slow enough to have the same spectra shape calculated for the decreasing and increasing field. We use the material parameters of Py as the experimental effects are more pronounced for Py in the perpendicular field geometry.

The spectra are calculated both for h-model and for ΔR-model and are represented in Fig. 4. Both models demonstrate the results qualitatively similar to the experimental measurements. Namely, for the larger particles the number of the resonances increases with the effective film thickness, reach the maximum at $h = 2\Delta R \approx 60$nm and then decreases. Nevertheless, this behavior is more pronounced in the h-model. The position of the resonances is between 6 and 12 kOe similar to the experimental data (Fig. 2b and 4). It means that the used material parameters are more or less similar to that of the experimental samples. In the case of the small colloidal particles with $D = 120$ nm there are two resonances in thin film. With the film thickening the second resonance decrease its amplitude and even can disappear in the case of the R-model, like in the experiment. Therefore, we can conclude that that h-model is more appropriate for the larger particles while the system with the smaller period is better correspond to the R-model. This can be explained as follows The intercap exchange interaction plays the significant role in the system and it is larger for the smaller periods of the system [10]. It depends on the cap overlap and is better described by the R-model. In the case of the larger particles the interaction is less so the h-model is more appropriate. Intrinsically, the structure of the experimental sample is something between these two geometries. In any case, the both models demonstrated qualitatively similar spectra.

We also calculated the spatial distribution of the magnetization oscillations at the resonances. Fig. 5 represents such modes calculated for the h-model with D = 340 nm and h = 60 nm. In this case, the number of the resonances is the largest. For the other geometries, this number is less, but the mode structure is the same in general. The geometry changing leads to consistent disappearance of the higher more nonuniform modes (higher modes correspond to the less external resonant field values in Fig. 5). As the magnetization is not uniform in the sample, all its components M_x, M_y, M_z are nonzero. In Fig. 5 we represent the amplitude of the magnetization deviation from equilibrium. It is calculated as $\max|\mathbf{M}_{res}(t) - \mathbf{M}_0|$ integrated over vertical z-axis. Here $\mathbf{M}_0$ is the magnetization in the equilibrium state withoutrf-excitation. $\mathbf{M}_{res}(t)$ is the magnetization under rf-excitation. The regions of the sample where oscillations have the maximal amplitude are colored in black. To illustrate the dynamics of the oscillations we show the snapshots of the in-plane component of **M** deviation in the bottom row of the Fig. 5.

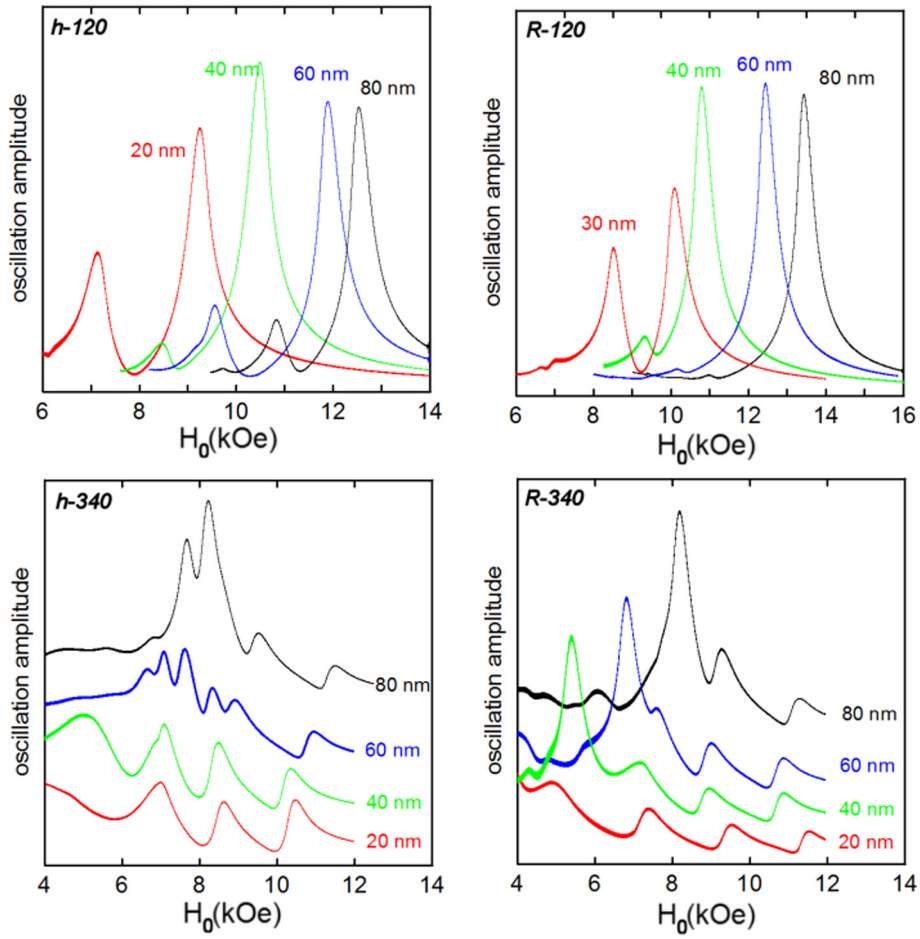

Fig. 4. Calculated spectra for hexagonal arrays of the Py nanocaps for different effective thicknesses of the magnetic covering. Top row: the particle diameter is 120 nm, bottom row: the particle diameter is 340 nm. Left column is for h-model, right is for ΔR-model. The DC field is perpendicular to the plane.

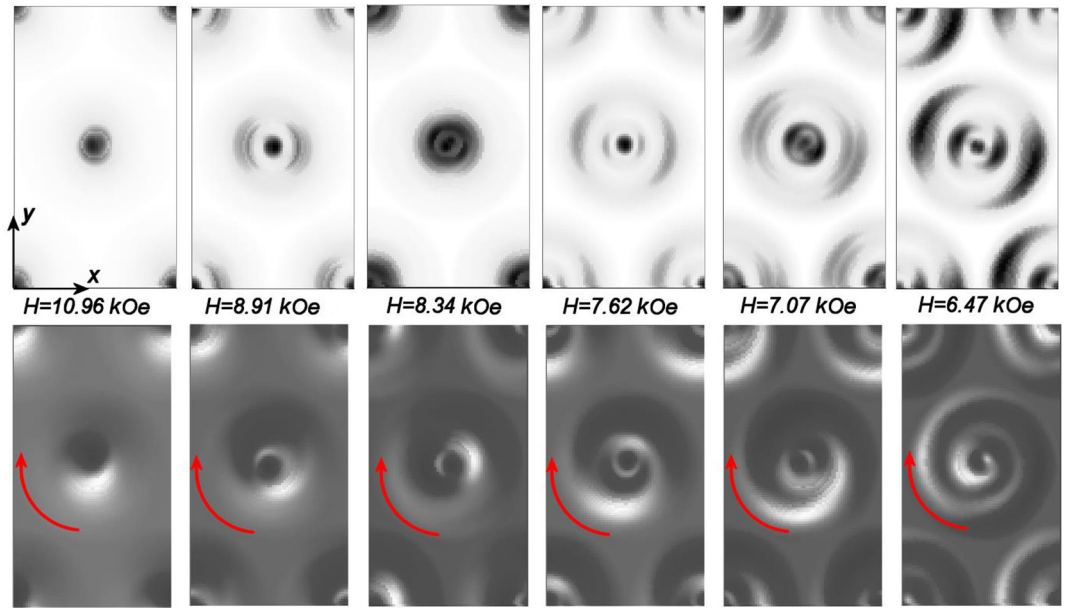

Fig. 5. At the top: the in-plane distribution of the FMR oscillation amplitude in the different modes for the perpendicular orientation of the DC external field. The darker areas correspond to antinodes of the corresponding mode. At the bottom: the snapshots of the in-xy-plane component of the deviation of the magnetization from its equilibrium. Lighter areas correspond to the larger magnetization deviation. The spiral structure of the higher modes is evident. During the period of the oscillation, the pictures made the complete revolution in clockwise direction (the view is from the top of the nanocap). The showed values of the magnetic field correspond to the resonant field values for 60 nm Py film on the top of 340 nm spheres. The corresponding movie is in the supplementary materials.

The first mode looks like the oscillations of the magnetization near the top of the nanocap. With the decrease of the field, peripheral regions become involved in the oscillations. The higher modes look like the spiral spin waves making clockwise revolutions. So, in the simulations we observe nonequivalence of the propagation of spin wave excitations in clockwise and counterclockwise direction, which is the sign of the nonreciprocity of the system. The possible nature of this nonreciprocity will be discussed below.

6. In-plane external field configuration

In the case of the in-plane external magnetic field orientation, the situation is quite different for the simulation. As the surface of the colloidal crystal is polycrystalline, the DC in-plane external magnetic field has different orientations with the respect to the crystal axes for different crystallites in the experiment. The value of the effective magnetic field depends on this orientation, therefore the FMR spectra should be different for different crystallites. To take into account this fact it is necessary to simulate the spectra for all possible orientations of the external magnetic field in plane in the range 0°–30° in the respect to the y-axis and average them.

Actually, we cannot carry out such numerical simulation for all samples due to enormously large computing time, which is necessary for such calculations. The example calculations are made for the system with D = 120 nm, 2ΔR = 60 nm. The spectra for averaging in the 0°–30° angle range are calculated with the step of 3.75°. The averaging demonstrates the broadening of the resonances due to such averaging (Fig. 6c). For other sample geometries we simulate the special case when the external magnetic field is directed along *y*-axis of the system ($\mathbf{H}_0 = H_0\mathbf{y}_0$, Fig. 3a) to have some ideas about the possible resonance modes in the in-plane field configuration.

The high frequency field is still oriented along *x*-axis ($\mathbf{H}_{rf} = H_{rf}\mathbf{x}_0$). The simulated system has the same geometrical parameters as in the case of the perpendicular field orientation. We use the material parameters corresponded to the Co here as the effects of the nanostructuring are more pronounced for the Co films in the in-plane DC field configuration in the experiments. The magnetic anisotropy is omitted again. The better coincidence with the experimental data is obtained for ΔR-model in this case; the calculated spectra are represented in Fig. 6a,b. We observe the increase in the peak numbers with the increase of the structure period and the magnetic film thickness like in the experiment. The structures of the oscillation modes are represented in Fig. 6d,e for the system with D = 340 nm and $2\Delta R$ = 60 nm. Evidently, the higher resonant value of the external field corresponds to the less non-uniform mode. The magnetization oscillates primarily in the regions of

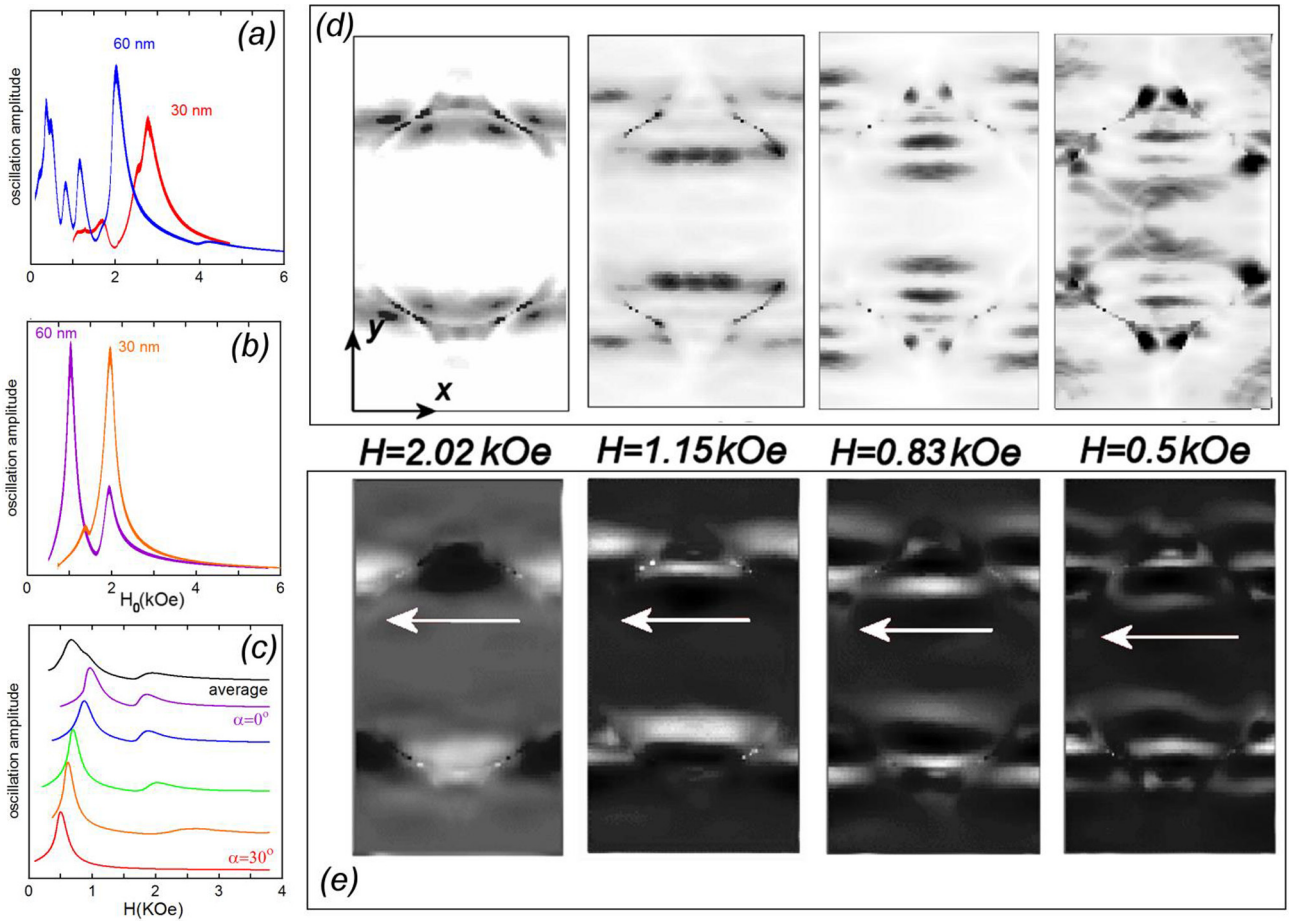

Fig. 6. At the left: spectra for hexagonal lattice of Co nanocaps for different effective thicknesses of the magnetic covering calculated for ΔR-model are represented. The DC field is directed in plane along y-axis. a) the particle diameter is 340 nm. b) The particle diameter is 120 nm. c) FMR spectra of the Co nanocaps (D = 120 nm, $2\Delta R$=60 nm) for different in-plain orientations of the static external field according to the y-axis. The represented curves are for the angles are 0°, 7.5°, 15°, 22.5°, 30°. The averaged spectrum is also shown (black line). d) The in-plane distribution of the FMR oscillation amplitude in the different modes for the in-plane orientation of the DC external field. The darker areas correspond to antinodes of the corresponding mode. f) The snapshots of the in-xy-plane component of the deviation of the magnetization from its equilibrium. Lighter areas correspond to the larger magnetization deviations. During the period of the oscillation the pictures made the one period shift in the left direction (the view is from the top of the nanocap). The arrow denotes the direction of the magnetization oscillation wave movement. The showed values of the magnetic field correspond to the resonant field values for 60 nm Co film on the top of 340 nm spheres. The corresponding movie is in the .

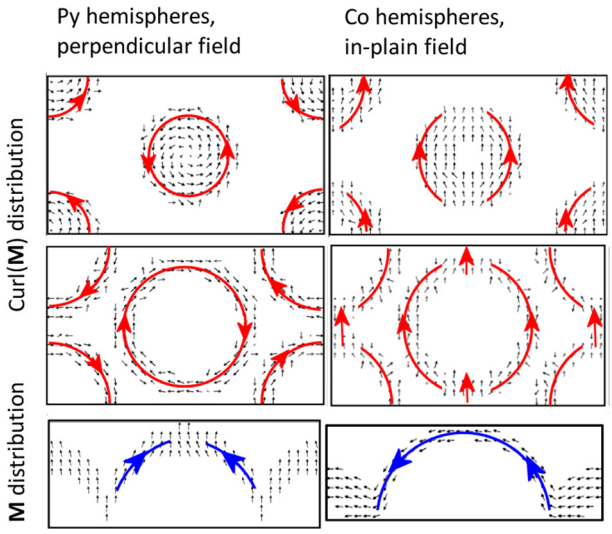

Fig. 7. The schematic distribution of the calculated field of the in-xy-plane component of the curl(**M**) in the system. Left column is for perpendicularly magnetized 340 nm Py nanocaps at 6.47 kOe. Right column is for in-plane magnetized 340 nm Co nanocaps at 0.5 kOe. Different xy-sections of the system are represented: top row is for z = 125, middle row is for z = 175 nm. The bottom row represents the magnetization distribution in the corresponding systems in yz-section.

the interparticle contacts in this mode. More non-uniform modes produce larger exchange fields, which decreases the resonance value of the constant external field. The decrease of the magnetic film thickness or the system period leads to the disappearance of the more nonuniform modes from the spectra. In the case of the in-plane orientation of the DC external field the nonreciprocity of the system leads to the nonequivalence of the propagation of spin waves in "forward"/"backward" direction along *x*-axis as it is represented in Fig. 6.

7. Discussion

What can be the reason of the nonreciprocity in the spin-wave oscillation rotation in the perpendicularly magnetized state or spin-wave propagation in the case of the in-plane magnetized state? The propagation of the electromagnetic wave can become nonreciprocal if some polar vector **c**, that also changes its sign under the time reversal, is present in the system. In this case, the frequencies of "forward"/"backward" waves (spin waves in our case) are split and $\Delta\omega \sim (\mathbf{kc})$, where **k** is the wave vector. Usually the toroidal moment of the magnetization distribution

$$\mathbf{T} = \frac{1}{V}\int [\mathbf{r} \times \mathbf{M}] dV$$

is used for phenomenological description of the nonreciprocity, for example, in the case of the light reflection [21] or optical second-harmonic generation [22]. Magnetization distribution is highly nonuniform in our system. In this case, a local analog of toroidal moment is curl(**M**) which has the same symmetry with respect to time and spatial reversal. In the case of the rotation the φ-component of curl(**M**) enters the expression for the frequency splitting. The calculated distribution of the curl(**M**) in the system is schematically represented in Fig. 7. It is seen that in the case of the perpendicular field geometry the magnetization distribution has the φ-component of curl(**M**). Therefore, in these conditions the oscillations are not the standing waves, they travel making complete revolution around a nanocap during the period of the oscillation. The direction of rotation is selected by the magnetostatic interaction in this case similar to Damon-Eshbach waves (see [23]).

The same way in the case of the in-plane field geometry the magnetization distribution in the system has in plane component of curl(**M**). directed in x-direction perpendicularly to the external magnetic field. This leads to the nonequivalence of the propagation of waves along *x*-axis. Evidently, it is the curvature of the surface of the magnetic layer forming the nanocap that leads to nonuniform magnetization distribution with the nonzero curl(**M**). To be sure, we also carried out the simulations for the regular hexagonal lattice of the contacting flat Py discs (the diameter is 340 nm and the thickness is 10 ÷ 60 nm). We do not find out nonreciprocity in the FMR oscillations in this case.

We also should discuss the comparability of our experimental results and the results of the numerical simulations here. Our simulations do not aim for a quantitative comparison with the experiment because of the following reasons. The accuracy of the particle diameter measurements is 10%, the same is the accuracy of the manufactured film thickness in the magnetron sputtering process. Also, the material parameters used in the simulations correspond to the material parameters of the bulk materials, while the magnetization and exchange constant in the thin films on the surface of the PMMA probably differ. Therefore, while the position and the amplitude of the individual resonance can be different in the simulation and the experiment, their overall position is the same. For example, resonances of the Py samples lie in the range of 6–12 kOe for the perpendicular external field both in the experiment and in simulations. In addition, we experimentally observe

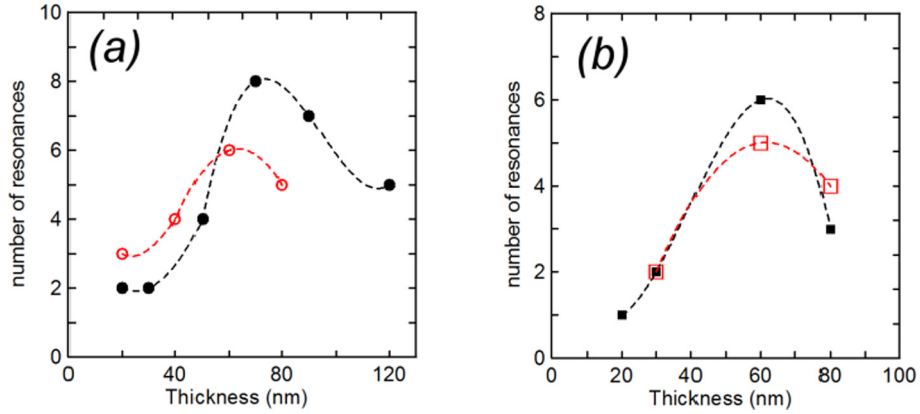

Fig. 8. The number of resonances in the FMR spectrum of the magnetic film on the top of the colloidal crystal (D = 340 nm) as a function of the film thickness. Black solid circles or squares are the experimental data, red opened circles and squares are the data of the micromagnetic simulations. The dashed lines are guides for eyes. a) is for Py nanocaps in the perpendicular external field. b) is for Co nanocaps in the in-plain external field.

and obtain in simulations similar dependency of the resonances number on the film thickness (Fig. 8). As our simulations demonstrate, the geometry of the magnetic coating of the colloidal particles influences the position and even on the number of the resonances. In any case, the FMR modes demonstrate their nonreciprocal character as the surface is hemispherical and the magnetization distribution have the nonzero in-plane component of the curl(**M**). The micromagnetic simulations show that peculiarity of the FMR modes in the system.

8. Summary

The 2D hexagonal lattices of contacting magnetic (Co and permalloy) nanocaps exhibit series of the resonance peaks in the FMR spectra which is absent in the case of the flat magnetic film of the same materials. The number of peaks increases with the magnetic layer thickness ($20 \div 60$ nm) and lattice period ($120 \div 340$ nm). The micromagnetic modeling of the system demonstrates all experimentally observed peculiarities of the spectra. The calculated modes of the ferromagnetic oscillations of the system have the form of the nonreciprocal spin waves. The nonequivalence of the propagation of the waves is caused by the toroidal moment of the magnetization distribution in the system.

Acknowledgments

The experimental investigations were supported by the Russian Foundation for Basic Research (RFBR) (Grant Nos. 15-02-03046). The magnetic simulations were supported by the Russian Science Foundation (Grant No. 16-12-10254).

Appendix A. Supplementary data

Supplementary data associated with this article can be found, in the online version, at https://doi.org/10.1016/j.jmmm.2017.09.082.

References

[1] S.O. Demokritov, A.N. Slavin, Magnonics From Fundamentals to Applications, Springer-Verlag 2013 ISSN 0303-4216.
[2] R. Streubel, P. Fischer, F. Kronast, V.P. Kravchuk, D.D. Sheka, Y. Gaididei, O.G. Schmidt, D. Makarov, J. Phys. D: Appl. Phys. 49 (2016) 363001.
[3] P.A. Kolodin, B. Hillebrands, J. Magn. Magn. Mat. 161 (1996) 199–202.
[4] V. Castel, J. Ben Youssef, F. Boust, R. Weil, B. Pigeau, G. de Loubens, V.V. Naletov, O. Klein, N. Vukadinovic, Phys. Rev. B 85 (2012) 184419.
[5] S.V. Nedukh, S.I. Tarapov, D.P. Belozorov, A.A. Kharchenko, V.O. Golub, I.V. Kilimchuk, O.Y. Salyuk, E.V. Tartakovskaya, S.A. Bunyaev, G.N. Kakazei, J. Appl. Phys. 17B521 (2013).
[6] J.I. Martin, J. Nogues, K. Liu, J.L. Vicent, I.K. Schuller, J. Magn. Magn. Mater. 256 (2003) 449.
[7] J.Q. Liu, A.I. Maaroof, L. Wieczorek, M.B. Cortie, Adv. Mater. 17 (2005) 1276.
[8] M. Albrecht, G. Hu, I.L. Guhr, T.C. Ulbrich, J. Boneberg, P. Leiderer, G. Schatz, Nat. Mater. 4 (2005) 203.
[9] T.C. Ulbrich, D. Makarov, G. Hu, I.L. Guhr, D. Suess, T. Schrefl, M. Albrecht, Phys. Rev. Lett. 96 (2006) 077202.
[10] M.V. Sapozhnikov, O.L. Ermolaeva, B.G. Gribkov, I.M. Nefedov, I.R. Karetnikova, S.A. Gusev, V.V. Rogov, B.B. Troitskii, L.V. Khokhlova, Phys. Rev. B 85 (2012) 054402.
[11] R. Streubel, D. Makarov, F. Kronast, V. Kravchuk, M. Albrecht, O.G. Schmidt, Phys. Rev. B 85 (2012) 174429.
[12] R. Streubel, F. Kronast, C. F. Reiche, T. Muhl, A.U.B. Wolter, O.G. Schmidt, D. Makarov, Appl. Phys. Lett. 108 (2106) 042407.
[13] J. Sklenar, P. Tucciarone, R.J. Lee, D. Tice, R.P.H. Chang, S.J. Lee, I.P. Nevirkovets1 O. Heinonen, and J. B. Ketterson, Phys. Rev. B 91 (2015) 134424.
[14] M.V. Sapozhnikov, S.A. Gusev, V.V. Rogov, O.L. Ermolaeva, B.B. Troitskii, L.V. Khokhlova, D.A. Smirnov, Appl. Phys. Lett. 96 (2010) 122507.
[15] R. Naik, C. Kota, J.S. Payson, G.L. Dunifer, Phys. Rev. B 48 (1993) 1008.
[16] P.K. Tannenwald, R. Weber, Phys. Rev. 121 (1961) 715.
[17] A. Martins, F. Pelegrini, M.M. Soares, F. Garcia, J. Magn. Magn. Matt. 327 (2013) 44.
[18] M.J. Donahue, D.G. Porter, OOMMF User's Guide Version 1.0, National Institute of Standards and Technology, Gaithersburg, MD, 1999.
[19] E.D. Boerner, H.N. Bertran, I.E.E.E. Trans, Magn. 33 (1997) 3052.
[20] A.A. Fraerman, I.M. Nefedov, I.R. Karetnikova, M.V. Sapozhnikov, I.A. Shereshevskii, Phys. Met. Metallogr. 92 (supplementary issue 1) (2001) 226.
[21] O.G. Udalov, M.V. Sapozhnikov, E.A. Karashtin, B.A. Gribkov, S.A. Gusev, E.V. Skorohodov, V.V. Rogov, A.Y. Klimov, A.A. Fraerman, Phys. Rev. B 86 (2012) 094416.
[22] B.B. Van Aken, J.P. Rivera, H. Schmid, M. Fiebig, Nature 449 (2007) 702.
[23] R.W. Damon, J.R. Eshbach, J. Phys. Chem. Solids 19 (1961) 308.